Acta Materialia 148 (2018) 202–215

Contents lists available at ScienceDirect

Acta Materialia

journal homepage: www.elsevier.com/locate/actamat

Full length article

Longitudinal twinning in a TiAl alloy at high temperature by *in situ* microcompression

Thomas Edward James Edwards [a, *], Fabio Di Gioacchino [a], Gaurav Mohanty [b], Juri Wehrs [b], Johann Michler [b], William John Clegg [a]

[a] Department of Materials Science and Metallurgy, 27 Charles Babbage Rd, University of Cambridge, Cambridge CB3 0FS, UK
[b] Empa, Swiss Federal Laboratories for Materials Science and Technology, Laboratory for Mechanics of Materials and Nanostructures, 3602 Thun, Switzerland

ARTICLE INFO

Article history:
Received 29 August 2017
Received in revised form
4 December 2017
Accepted 15 January 2018
Available online 3 February 2018

Keywords:
Titanium aluminides
Micromechanics
Electron backscattering diffraction (EBSD)
Digital image correlation
Deformation twinning

ABSTRACT

The stress required to activate twinning of the longitudinal $<11\bar{2}]\{111\}$ system in the lamellar γ-TiAl phase of the alloy Ti-45Al-2Nb-2Mn (at.%)-0.8 vol.% TiB_2 was measured at several temperatures up to 700 °C by *in situ* micropillar compression of soft mode oriented γ-TiAl/α_2-Ti_3Al lamellar stacks. The lamellae undergoing deformation twinning were identified by electron backscatter diffraction orientation mapping. In some cases, such lamellae were not constrained by domain or colony boundaries and longitudinal twinning was the only deformation mechanism observed based on digital image correlation strain maps. The resolved shear stress for such unconstrained twinning was found to increase monotonically with temperature from 25 °C to 700 °C. This is consistent with the stacking fault energy increasing with temperature as found in many metallic alloys, suggesting that the increased ease of deformation twinning at high temperature in bulk TiAl alloys is due to the increased ease with which the twinning shear can be accommodated by the neighbouring domains and lamellae with increasing temperature, rather than a thermal softening of the intrinsic twinning mechanism.

1. Introduction

Twinning in TiAl alloys is essential for sufficient ductility to be obtained [1]. Twinning of the γ-TiAl phase in dual-phase lamellar TiAl alloys is known to occur as both longitudinal and transverse modes of the same $<11\bar{2}]\{111\}$ [1] system [2,3], where the twins shear either parallel or transversal to the interfacial planes, respectively. Twinning is reported to operate more easily with increasing temperature in both equiaxed γ-TiAl grains and lamellar colonies [3–5]. The ease of twinning in γ-TiAl can also be increased by reducing the Al content and alloying with Mn and Nb [3].

The onset of twinning requires the formation of a twin interface stacking fault [6]; in γ-TiAl the stacking fault maintains nearest neighbour bonding and no shuffle is required for mechanical twinning [7,8]. Ab-initio calculations have determined the twin interface stacking fault energy to be approximately half the superlattice intrinsic stacking fault (SISF) energy [9,10]. Measurements of the SISF energy by transmission electron microscopy weak beam imaging of dissociation lengths between superdislocation partials on TiAl alloys of varying Al and Nb content [11,12], as well as atomistic modelling by density functional theory [13], showed a reduction of the twin interface stacking fault energy as a result of alloying, consistent with the observation that the stress for the operation of mechanical twinning depends on the Al and Nb content. Once nucleated, twin propagation in γ-TiAl occurs by the passage of Shockley partial dislocations along the interface [14]. A pole mechanism has been observed by *in situ* imaging of twinning to generate Shockley partials on successively stacked $(111)_\gamma$ planes; this requires the dissociation of an ordinary dislocation into a Shockley and a Frank partial [15,16]. The Shockley partial spirals up the pole; this occurs by glide. However, the nucleation of the pole requires the Frank partial segments to expand by climb; having a Burgers vector of 1/3[111], they are sessile on {111} and {100} planes. It is often thought [3] that such climb being thermally activated, this should lead to twinning in γ-

* Corresponding author.
E-mail addresses: teje2@cam.ac.uk (T.E.J. Edwards), fd302@cam.ac.uk (F. Di Gioacchino), gaurav.mohanty@empa.ch (G. Mohanty), juri.wehrs@empa.ch (J. Wehrs), johann.michler@empa.ch (J. Michler), wjc1000@cam.ac.uk (W.J. Clegg).

[1] This notation is employed to reflect the tetragonal symmetry of γ-TiAl; $<11\bar{2}]$ indicates that the first two indices are permutable, but the third is not.

https://doi.org/10.1016/j.actamat.2018.01.007

TiAl occurring more readily at higher temperature, as observed.

In f.c.c. metals, the SISF energy increases with temperature [17,18], suggesting the twinning stress should also increase with temperature. Unambiguous measurement of the temperature dependence of the critical resolved shear stress (CRSS) for mechanical twinning of f.c.c. metals is complicated by the increasing ease of dislocation glide, particularly at higher temperature. However, in systems such as both the disordered b.c.c. and ordered $D0_3$ structures of Fe-25Be (at.%) [19], amongst others [6,20–22], twinning can be obtained in certain single crystal orientations, and hence the critical resolved shear stress for twinning can be measured independently of slip. In such systems the resolved shear stress required for the onset of twinning increases with temperature. To date, no extensive studies on the temperature dependence of the stacking fault energies, or the CRSS for twinning in γ-TiAl, longitudinal or other, have been undertaken; however, Yoo and Fu [8] have proposed that the temperature dependence of the SISF energy in γ-TiAl may affect the occurrence of twinning.

Recently, microcompression was employed [23] to measure the resolved shear stress required to activate longitudinal twinning in soft-mode oriented colonies, where the lamellae extended the full pillar width and twinning was hence not constrained by domain or colony boundaries. This required the use of pre- and post-test crystal orientation mapping to determine which lamellae in the pillars had undergone longitudinal twinning in contrast to the many grown-in twins. This was because longitudinal mechanical twins in γ-TiAl have parallel twin interfaces [24], like annealing twins. In addition, when pillars were selectively milled [23] to instead contain domain boundaries, the twinning stress nearly doubled, such that the effect of constraint by surrounding lamellar domains was a further complication in determining the reason for mechanical twinning being facilitated at higher temperatures.

The aim of this paper is to understand the reason for this increasing ease of operating twinning. To do this, lamellar stacks of Ti-45Al-2Nb-2Mn (at.%)-0.8 vol.% TiB_2 were microcompressed *in situ* at several temperatures up to 700 °C. The temperature dependence of the resolved shear stress for the onset of unconstrained longitudinal twinning was hence determined. The results were compared with findings from a parallel study on the temperature dependence of the occurrence of longitudinal twinning in bulk polycrystalline nearly lamellar compression testpieces of the same alloy, to develop a mathematical formulation of the temperature dependence of the onset stress for both unconstrained and constrained longitudinal twinning of γ-TiAl.

2. Experimental procedures

2.1. Material and metallographic preparation

Cuboidal microcompression specimens, $5 \times 5 \times 11\ \mu m^3$ in size, were produced in single colonies of commercial TiAl alloy Ti-45Al-2Nb-2Mn (at.%)-0.8 vol.% TiB_2 in a nearly lamellar condition following centrifugal casting and HIPping, by Ga^+ focussed ion beam (FIB) milling in a scanning electron microscope (SEM) (Helios NanoLab, FEI, USA), as in Fig. 1(a). The micropillars were located close to a sample edge, as described elsewhere [23]. A summary of the measured alloy composition and the microstructural dimensions of the alloy condition are given in Tables 1 and 2 respectively.

2.2. Mechanical testing

Micromechanical testing was undertaken using a 10 μm diameter diamond flat punch (Synton-MDP AG, Switzerland) at temperatures up to 700 °C using an Alemnis high temperature nanoindenter (Alemnis AG, Switzerland) [25,26], which utilizes independent sample and compression tip heating. The upper envelope of achievable temperatures previously reported for *in situ* micromechanical testing [26] was extended by improving the design of the miniaturised resistance heaters. Samples were cemented using an electrically conductive adhesive (Pyro-Duct 597-A, Aremco, USA) and cured in air (80 °C, 30 min). To minimise oxidation of the micropillars, the SEM chamber was pumped and then purged with Ar three times before heating the sample and tip. There exists a temperature gradient between the diamond tip and the temperature measured by the indenter thermocouple. This temperature gradient was determined as a function of test temperature for the flat punch indenter by performing calibration indents on a copper sample stub with an embedded K-type thermocouple - prior to testing the TiAl alloy; such calibrated values may deviate from the actual tip temperature by up to 8 °C. Tip-sample surface temperature calibration up to 700 °C on the TiAl sample was undertaken in two stages. First, a coarse temperature tuning was made by indenting the TiAl sample surface with a load hold at 50 mN, and minimising the temperature change of the tip upon contact as reported in Ref. [25]. This was followed by a fine tuning step in which the tip was held at constant position, akin to a relaxation test at very low loads, for 600 s after the sample was unloaded from 50 mN to 5 mN, and the load drift rate was minimised. It should be noted that the Alemnis indenter is displacement controlled, hence constant position corresponds to a constant depth experiment [27]. Both these calibrations were performed in constant power heating mode for the sample and the indenter. A technical note concerning the impact of the low conductivity of TiAl and radiation effects on temperature tuning above 600 °C is given in Appendix A.

Initial contact with the pillars for punch alignment and contact surface determination did not exceed a load of 50 μN. In order to achieve good SEM imaging to see the alignment, it was necessary to set the cage on the Everhart-Thornley detector to a strong negative bias in order to repel thermal electrons emitted from the sample. This, combined with oversampling by line integration, greatly improved the image quality at 700 °C. In the majority of cases, the top surfaces of the pillars displayed no evidence of misalignment with the diamond punch when imaged in the SEM at room temperature. Any pillars that showed signs of misalignment were excluded.

The micropillar compression tests were carried out in displacement controlled mode at a displacement rate of $0.05\ \mu m\ s^{-1}$ (giving a strain-rate ~$4 \times 10^{-3}\ s^{-1}$). The sample was strained to a displacement of 1.2 μm (before correcting for the frame compliance), after which the sample was unloaded. The unloading was paused at constant a displacement value corresponding to ~2 mN and the load drift rate measured to ensure it was low, and to perform corrections to the loading curve where necessary, Fig. 2(a). The magnitude of the load drift rate rarely exceeded $10\ \mu N\ s^{-1}$ (cumulative load drift of less than 4% of the maximum load in most cases). For compression testing, the sample and indentation tip heaters were operated at constant power.

At the end of the unloading sequence, the first four pillars tested at 700 °C remained attached to the punch and were hence loaded in tension, to a maximum stress of 67 MPa before releasing, Fig. 2(b). Such tensile loading did not occur in the remaining pillars tested at 700 °C; similarly this was not observed in tests below 700 °C. It is possible that a reaction compound formed at the punch-pillar interface at 700 °C, causing the punch to remain attached to the top of the pillar after unloading. The eventual tensile stress as unloading progresses further is too low to have any effect of significance on the plasticity of the pillars. However, an interfacial compound may increase the punch-pillar friction, resisting lateral

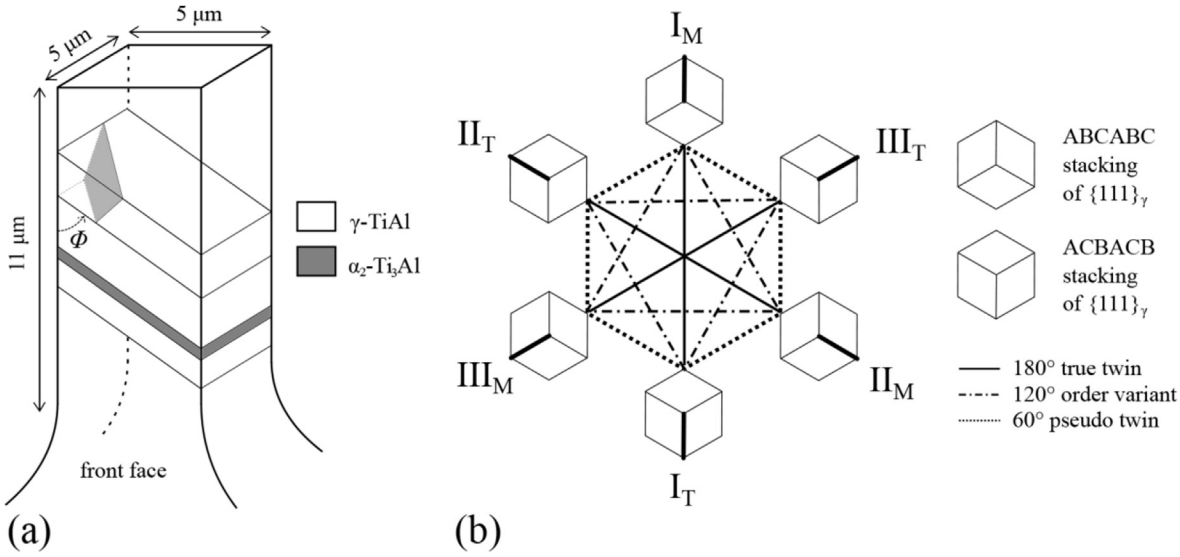

Fig. 1. (a) Drawing showing the angle Φ between lamellae and the pillar axis, and the potential orientation of a domain boundary, light grey, into the pillar depth. (b) schematic of the crystallographic relationship and nomenlature between the six possible face-centred tetragonal γ-TiAl orientation variants; the plane of the drawing is parallel to the $(0001)_{\alpha 2}$ basal plane of the α_2-Ti_3Al phase coexisting in a same lamellar colony; the thickest black lines on the cube projections along $(111)_\gamma$ indicate the c-axis direction; adapted from Ref. [59].

Table 1
Nominal and measured compositions of the titanium aluminide alloy studied according to ASTM standards E2371, E1409, E1447 and E1941. Note that the boron content in Ti4522XD exceeds the maximum measurable by ASTM E2371.

	Ti/at.%	Al/at.%	Nb/at.%	Mn/at.%	TiB_2/vol. %	O/at.%	N/at.%	C/at.%	H/at.%	Mo, Cu, Si, Fe, Ni, Cr, W, Co, V, Sn, Bi, Pb, Zr, P/at.%
Nominal	bal.	45	2	2	0.8	0	0	0	0	0
Measured, matrix only (TiB_2 excluded)	bal.	44.7	1.8	1.8	–	0.21	0.05	0.03	0.04	≤0.01

Table 2
Microstructural dimensions of the Ti-45Al-2Nb-2Mn(at%)-0.8 vol% TiB_2 (Ti4522XD) alloy, obtained from BSE images (colony size) and EBSD maps (lamellar dimensions).

Colony size/μm	α_2 fraction	Mean γ lamellar thickness/μm	Mean α_2 lamellar thickness/μm	Mean γ domain length/μm
70	9.5%	1.4 ± 0.9	0.26 ± 0.09	9.7

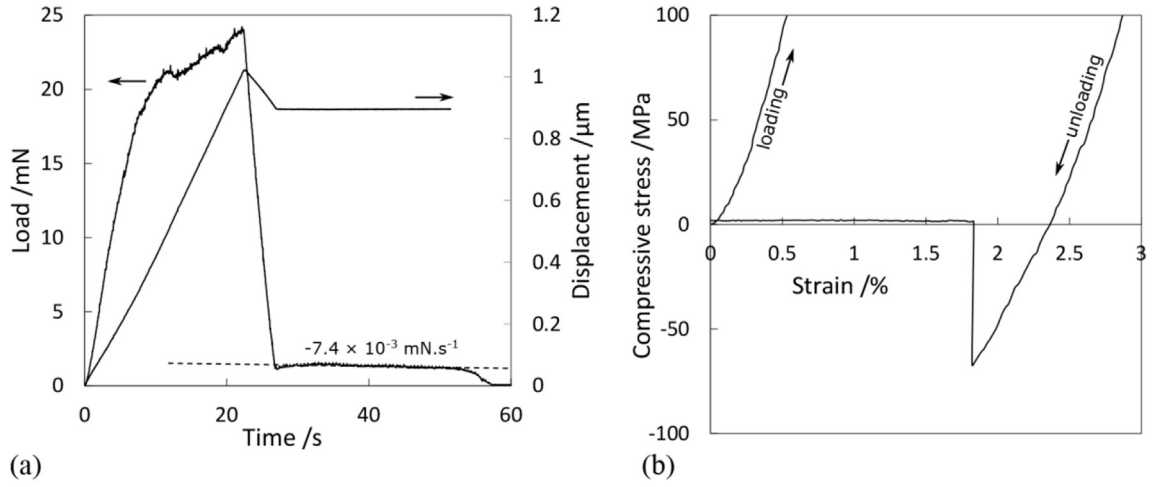

Fig. 2. Loading procedure: pillars were loaded in displacement control according to the (rig compliance corrected) scheme in (a); the load response, (a), indicated low thermal drift. Upon unloading the first few pillars at 700 °C, a tensile region was measured (b). Note that loading in (b) was expressly performed to a lower strain level than the majority of pillars in the present study.

translation of the top of the pillar during loading and resulting in an apparent hardening [28]. Nevertheless, no such diffusion bonding was detected at 367 °C or 633 °C in the loading curves, hence any trends in the temperature dependence of deformation mechanisms reported in section 3.1 are unaffected by any interfacial compound formation up to 633 °C, despite any potential overestimates of stresses achieved at 700 °C.

2.3. Identification of longitudinal twinning and measurement of CRSS

The crystal orientations of the lamellae and their angle to the loading axis, Φ, at the exposed side face of the pillars, Fig. 1(a), were determined by electron backscatter diffraction (EBSD) (NordlysNano, Oxford Instruments, UK) on the FIB/SEM, similarly to [23], both before and after compression. The occurrence of longitudinal twinning in one or two γ-TiAl variants in a pillar was identified by comparison of the two EBSD maps, using a method previously reported for room temperature tests [23]. The nomenclature for the γ-TiAl variants is explained in Fig. 1(b).

2.4. Mapping of surface strain

Surface strain mapping of the exposed side face of the pillars was achieved by digital image correlation (DIC) of a Pt speckle pattern that was electron beam deposited following pre-test EBSD mapping, as in Refs. [23,29]. Alternative speckling methods for high temperature, high resolution DIC (HRDIC) [30,31] were found to be unsuited to the present micropillars. The Pt pattern was imaged by both secondary and backscatter electron imaging perpendicular to the pillar face after exposure to temperatures up to 700 °C, Fig. 3(b,e). The importance of using optimised pattern deposition conditions is shown in Fig. 3(a and b) where the initially poorly deposited pattern at the pillar base deteriorates to an unusable state upon thermal exposure. The identification of deposition conditions for the Pt speckle pattern, Table 3, that enabled good thermal stability by ensuring that the Pt islands were suitably isolated to limit migration [31], was crucial to successful strain mapping of the pillar side surface up to 700 °C. The benefit of using Pt as the speckling element is illustrated in Fig. 3(e) in which the use of backscatter electrons imaging increases the compositional contrast of the speckle pattern relative to the underlying TiAl. This limits the oxide-related diffuse smearing of the speckles seen in secondary electron imaging Fig. 3(b) after high temperature compression.

To quantitatively demonstrate the suitability of the electron beam-deposited Pt speckle pattern for high temperature testing, and give an upper bound to the noise resulting from the combination of pattern instabilities and imaging conditions, some dummy regions of the samples underwent equivalent ion beam preparation and pattern deposition steps as the pillars themselves, but were not mechanically tested. Correlation of the same dummy region imaged before and after thermal exposure at 700 °C indicated an average noise level in the maximum shear strain measured per subset of $0.7 \pm 0.4\%$. This is to be compared with the equivalent average error resulting solely from imaging error, obtained by correlating a repeatedly imaged region that had not been thermally exposed. With the current setup, this baseline imaging error in maximum shear strain measurement was determined to be $0.6 \pm 0.3\%$, such that the increase in the error resulting from thermal exposure of the speckle pattern is minor. Such noise levels were well suited to the identification of the shear strain of micro slip bands. Throughout this study, DIC of pre- and post-deformation images was performed equivalently to [23] with a subset size of 16×16 px^2, giving a resolution of 108×108 nm^2, using a 25% overlap.

3. Results

The present study reports the first high temperature *in situ* SEM microcompression test of TiAl. Furthermore, it employs both EBSD crystal orientation and DIC strain mapping methods to measure the onset stress of a specific deformation mechanism. The loading curves for a representative selection of the pillars from each temperature are given in Fig. 4, illustrating the variability in loading behaviour observed for differing Φ and temperature conditions. For all micropillars tested in the present study, the yield stress at a strain of 0.2% was measured. All the data obtained are given in Fig. 5, and plotted against the lamellar orientation, along with that from a recent room temperature microcompression study on the same alloy [32] where the lamellar thickness was 287 nm for the γ-TiAl phase, so considerably reduced compared with 1.2 μm in the current work.

3.1. Temperature dependence of longitudinal twinning

The images of the pillar speckle patterns taken before and after compression at all temperatures were correlated to produce DIC strain maps as in Fig. 3(a–c). This identified the regions where plastic deformation was localised within the pillars. By measuring the changes in lattice orientation, using EBSD, to identify lamellae deforming by twinning, it was possible to select just the *N* pillars at each temperature where the deformation identified by strain mapping had occurred only by longitudinal twinning, as in Fig. 6(a and b). This group of pillars, summarised in Table 4, was used to determine values for the CRSS of longitudinal deformation twinning in Ti4522XD at 367, 633 and 700 °C, Fig. 6(a–f), by an identical method to [23]. The remainder of the pillars deformed by dislocation glide instead of twinning, e.g. Fig. 3(d–i), and displayed narrow bands of high shear strain along the slip plane, in contrast to the much wider regions of longitudinal twinning. Furthermore, the loading curves of pillars that deformed entirely, or at least in part, by conventional slip were highly serrated (the red curve in Fig. 4(a) corresponds to the pillar in Fig. 8(a – c), and the black one in Fig. 4(b) to the pillar in Fig. 3(d–i)).

Within the experimental spread for the, albeit now reduced, dataset, an increasing resolved shear stress is found to be required to activate longitudinal twinning as temperature increases, Fig. 7. Additionally plotted is the room temperature data obtained previously by the authors [23] and also a value from Fujimura et al. [33] for deformation twin operation on the same system at room temperature in a single crystal micropillar of γ-TiAl.

At all temperatures, the morphology of longitudinal twins was the same as that reported at room temperature [23]: the twins were not lenticular in shape. Instead, the sides were approximately parallel to the lamellar interfaces, with the longitudinal twins stretching the full pillar width, initiating on the lamellar interfaces of the parent and then growing across the full width of the lamella.

3.2. Effect of domains on longitudinal twinning

In some soft-mode pillars that displayed mechanical twinning, EBSD showed the presence of a domain boundary along the twinning lamella. This increased the RSS for twinning, see Fig. 8(a and b) which shows a pillar compressed at 367 °C; the RSS for twin operation at 367 °C in this case was measured to be 171 MPa, which is greater than the value of 123 ± 21 MPa for unconstrained longitudinal twinning at 367 °C in Fig. 7. Further, it should be noted that this can only be a lower estimate for the RSS for twinning because the glide plasticity in the neighbouring lamella evident from strain mapping, Fig. 8(c), may have operated first.

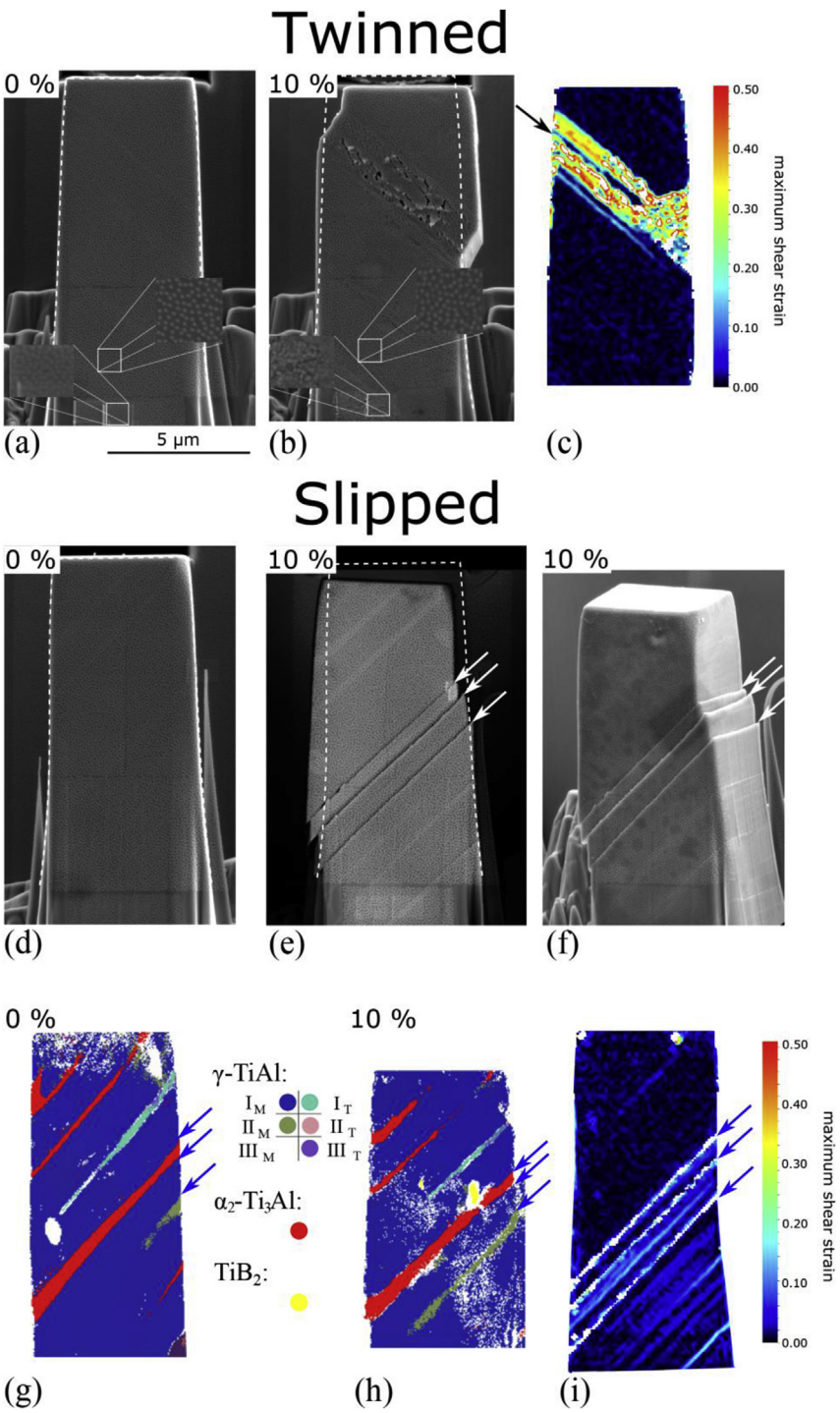

Fig. 3. (a,b) Secondary electron images before and after compression of the pillar in Fig. 6(a and b) compressed at 700 °C which underwent unconstrained longitudinal twinning, along with (c) the extracted strain map by digital image correlation. The equivalent analysis of a pillar undergoing deformation by slip upon compression at 633 °C is given in (d – f,i); major slip planes are arrowed in blue. The corresponding pre-/post-compression EBSD maps for this pillar are in (g,h): no mechanical twinning was measured. As previously reported [23], the shear strain of deformation twinning is sufficient to cause the rupture of the thin Ga^+ damaged surface layer upon which the Pt speckles locate, rendering strain measurements on the twin itself inaccurate. This is of no practical consequence to the conclusions drawn from the current work. (For interpretation of the references to colour in this figure legend, the reader is referred to the Web version of this article.)

Table 3
Electron beam deposition parameters for the high temperature stable Pt speckle pattern. The bitmap image for pattern deposition is given in Ref. [29].

Beam voltage/kV	Beam current/nA	Dwell time/ms.px^{-1}	Number of passes	Duration/s	Specified size of bitmap image/μm^2	Speckle particle diameter/nm
15	1.6	1.4	1	42	4 × 8	30

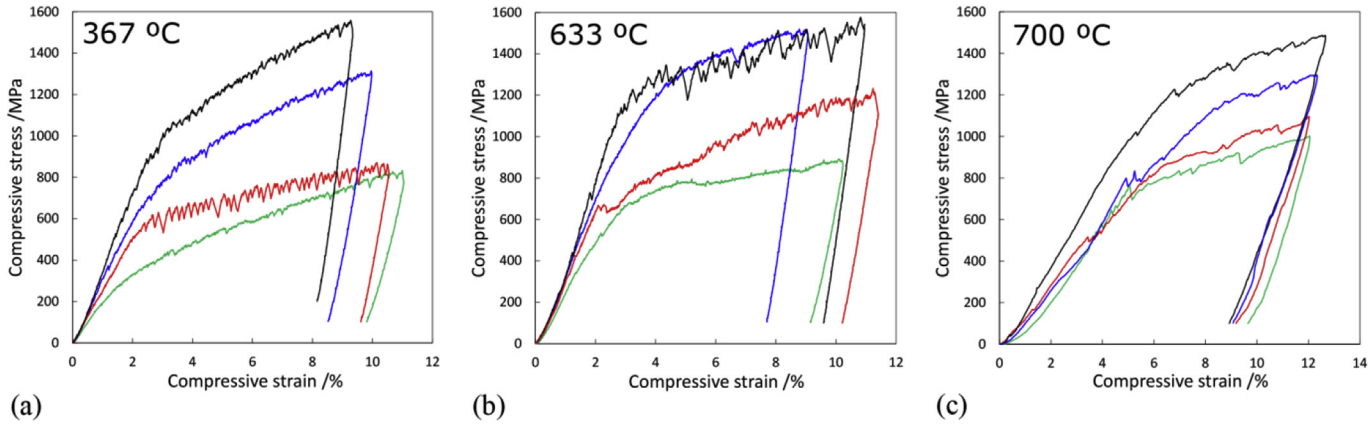

Fig. 4. (a–c) Examples of loading curves for the soft-mode pillars compressed at 367 °C, 633 °C and 700 °C, respectively, indicating both the extremes of loads attained and the varied degree of serration in the plastic region.

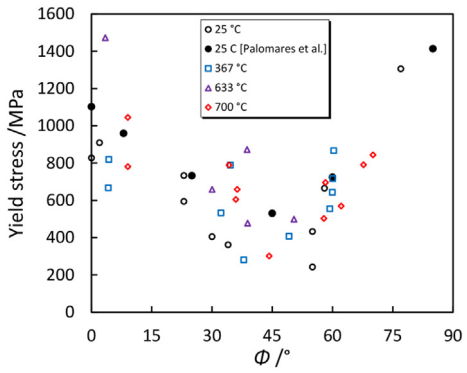

Fig. 5. Compressive yield stress of pillars as a function of angle Φ of the lamellae to the loading axis. A considerable spread in yield stresses is noted at each temperature, resulting from the range of Schmid factors, the specific combinations of γ-TiAl orientation variants present, and the eventual existence of domain boundaries and titanium diboride particles within the pillars.

3.2.1. Constraint by boride particles

Boride particles within pillars were also identified by crystal orientation mapping, Fig. 8(d), though the borides did not necessarily extend into the depth of the pillar parallel to the lamellar interfaces, as seen by comparing Fig. 8(d) and (e). A RSS of 149 MPa, higher than that measured in Fig. 7 for longitudinal twinning at 367 °C, was measured. However, boride particles were only identified to coincide with longitudinal twins in ~5% of the pillars tested.

4. Discussion

Classic studies on polysynthetically twinned (PST) crystals of model alloys [34,35], as well as later generation high Nb compositions [36], have demonstrated an unambiguous asymmetrical U-shape variation of the yield stress against lamellar orientation to the loading axis, Φ. However the angle Φ does not uniquely define a Schmid factor for a given longitudinal deformation mechanism, as the exact direction of slip or twinning in the slip/twin plane may also vary. If it is assumed that all six possible γ-TiAl variants exist in the single colony testpiece and are equally loaded, the ratio of the highest to lowest Schmid factor achievable for a longitudinal deformation system is 1.15. This corresponds to a ±30° in-plane rotation away from the direction of highest Schmid factor. Such an expected variation in the measured yield stress was evoked by Fujiwara et al. [34], where differing in-plane orientations of the crystals for a given Φ caused the U-curve to shift in stress. In the present work, the micropillars, like PST crystals, are constituted of single stacks of lamellae. However, as is visible in the crystal orientation maps, Fig. 6, all six γ-TiAl variants are regularly not present in the pillars due to the combination of lamellar thickness and specimen size employed. Hence an even greater variability in yield stress for a given Φ and temperature is expected, and indeed observed.

The reduced number of pillars compressed per lamellar orientation and temperature in the present study, due to the complexity of the experimental setup and deformation mapping methods, limits the extent to which an unambiguous trend in the variation of the U-curve with temperature can be determined. In addition, as will be discussed in section 4.2, the fact that some pillars include domain boundaries, or even boride particles, whilst in other pillars single domains stretch the full pillar width, further complicates any analysis. For the U-curve plot to be a useful method for describing the mechanical behaviour, samples should contain a sufficient number of lamellae for consistent results for a given Φ, as is the case for macroscopic PST crystals and micropillars with more refined lamellae than here. Hence, to better interpret the results of the present study, one must consider the effect of the microstructure of each pillar individually.

The serrated loading curves for pillars deforming by conventional slip is consistent with the observations of Chiu et al. [37] and Messerschmidt [38] et al. of dynamic strain ageing (DSA) in γ-TiAl; DSA was found to be most prominent at 500 °C and to be a result of dislocation core pinning by point defects; it has been suggested [38] that this is associated with antisite defects in such ordered structures (e.g. Ti on an Al site, Ti_{Al}). The lesser serration of the loading curves for pillars where deformation was attributed to twinning suggests that DSA is less effective on Shockley partial dislocations.

A recent size effect study on micropillars of the same alloy by Palomares et al. [32] at room temperature found the pillar size used here to be above the small size limit. Note that this does not necessarily imply that deformation twinning is not nucleation limited, as reported previously [23], and discussed below.

4.1. Temperature dependence of CRSS for unconstrained longitudinal twinning in lamellar γ-TiAl

Generally, thermally activated deformation mechanisms show a decreasing CRSS with increasing temperature [39]. However, here,

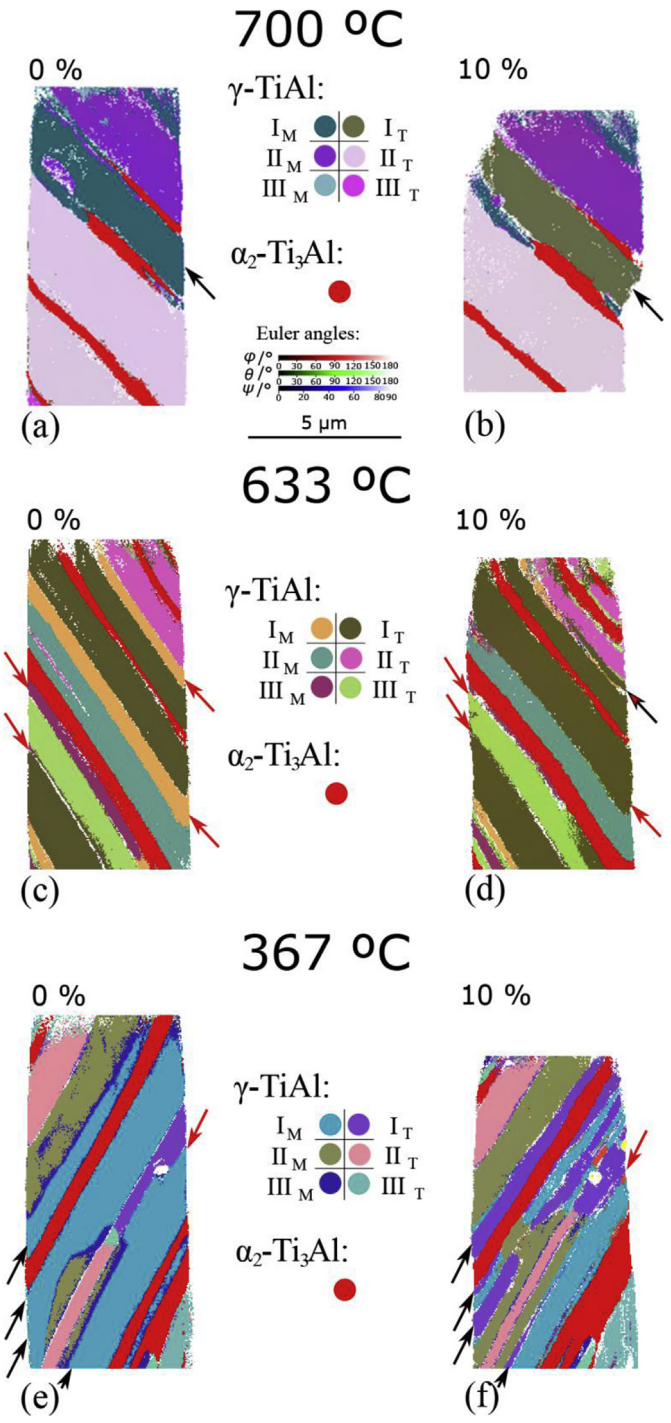

Fig. 6. (a–f) Example electron backscatter diffraction (EBSD) maps of crystal orientation in Euler angler colouring acquired before and after compression of soft mode pillars undergoing unconstrained longitudinal twinning at 700 °C, 633 °C and 367 °C. Arrowed in red are longitudinal twins that form with a parent lamella with a neighbouring true twin-oriented lamella already present; in black are those where a neighbouring true twin-oriented lamella is not. For an explanation of the nomenclature for γ-TiAl matrix-twin pairs and other pseudosymmetric variants see Fig. 1(b). (For interpretation of the references to colour in this figure legend, the reader is referred to the Web version of this article.)

we find that the stress for unconstrained longitudinal twinning increases with increasing temperature. Twinning in γ-TiAl, even in the longitudinal mode, is known to be mediated by the passage of Shockley partial dislocations [14] which, as explained earlier, propagate on successively stacked $(111)_\gamma$ planes via a pole mechanism for dislocation multiplication. The climb process necessary for expansion of the Frank partial dislocation segments is facilitated by an increased diffusivity with temperature, which is mediated by Ti_{Al} antisite defects rather than vacancies alone [14,40]. As a result, an increased tendency for mechanical twinning in γ-TiAl at higher temperatures has been associated in the literature with the climb of the Frank partials becoming easier [3].

To better understand the temperature dependence of the CRSS for unconstrained longitudinal twinning of γ-TiAl, a mathematical formulation of the twinning condition is sought. In 1965, Bolling and Richman [19] introduced an energetics model for the occurrence of continual mechanical twinning, where plasticity occurs almost entirely by the operation of deformation twinning. In fact, dislocation glide was estimated to have been responsible for only 1% of the total deformation. This model may be extended and applied to the current situation of longitudinal twins in lamellar γ-TiAl. First, like Bolling and Richman, let us consider the energy balance required for the increase in volume dV of a given twin. As they point out, though this approach would appear to assume a prexistent twin, it in fact encompasses both propagation and nucleation stages, the latter by simply reducing the twin size until common nucleation-based analyses of twinning emerge as a limiting case of the present analysis.

For twinning to occur:

$$\varepsilon_s \tau_a dV \geq \varepsilon_s \tau_0 dV + \gamma_T dA + \Delta f_v dV + \varepsilon_s \xi dV + \varepsilon_s \tau_D{}^T dV \qquad (1)$$

where the left hand side of the inequality is the external work done for the volume increment, with ε_s the twinning shear and τ_a the applied shear stress resolved onto the appropriate plane for the twin system considered. The first three terms on the right hand side of Eq. (1) relate to energy storage: $\varepsilon_s \tau_0 dV$ is the elastic energy stored, where τ_0 is a shear stress elastically resisting twin expansion. The second, $\gamma_T dA$, is the energy stored in the twin interface, with γ_T the specific surface free-energy of the twin. The term Δf_v was included by Bolling and Richman for generality; it is the change in specific volume free energy of the twin with respect to the matrix. It is relevant for cases such as where the twinning shear does not exactly restore the lattice in a simple mirrored configuration, such as in ordered materials like Fe_3Be. In the case of $\{111\}\langle 11\bar{2}]$ twinning in γ-TiAl, it is reasonably assumed that $\Delta f_v = 0$, the lattice being nominally perfectly restored, albeit mirrored [7,8]. Finally, the two last terms on the right hand side of Eq. (1) are dissipative; the first, $\varepsilon_s \xi dV$, relates energy loss as a consequence of twinning but by processes that are not intrinsic to it. In practice, this may be the operation of glide mechanisms both externally and internally to the twin to accommodate the twinning shear, at a CRSS τ_y, or the formation of micro-cracks. In γ-TiAl, both such mechanisms, $\{111\}\langle 1\bar{1}0]$ ordinary and $\{111\}\langle 10\bar{1}]$ super-dislocation motion [3,23], and micro-cracking [41], are reported to occur in the process zone ahead of twins. The last term, $\varepsilon_s \tau_D^T dV$, was not included by Bolling and Richman and has been added to relate the energy dissipated by the operation of twin-mediating dislocation mechanisms, intrinsic to twinning in γ-TiAl. τ_D^T is the critical resolved shear stress for the movement of such $\{111\}\langle 11\bar{2}]$ Shockley partial dislocations.

Following Bolling and Richman, we set: $\beta = \frac{1}{\varepsilon_s}\frac{dA}{dV}$, hence a condition for twinning may be written as:

$$\tau_a{}^T = \tau_0 + \gamma_T \beta + \frac{\Delta f_v}{\varepsilon_s} + \xi + \tau_D{}^T \qquad (2)$$

where τ_a^T is the applied resolved shear stress to activate the twin volume change dV. This energetic model for twin formation is

Table 4
Summary of micropillar populations per test temperature.

Temperature/°C	Total number of pillars tested, after exclusions as per section 2.2	Number of soft-mode pillars displaying unconstrained longitudinal twinning, *N*
25 [23]	10	6
367	10	3
633	7	3
700	11	5

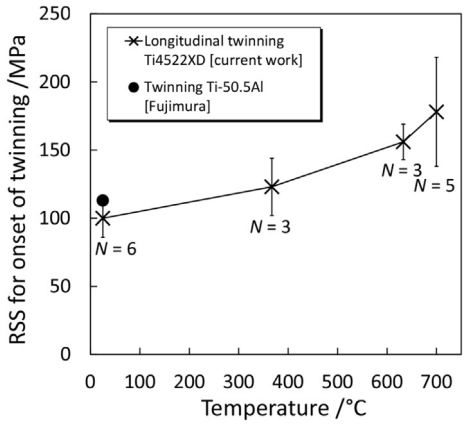

Fig. 7. Measured average resolved shear stresses for the onset of unconstrained longitudinal twinning as a function of temperature.

therefore fundamentally equivalent, in the physical processes it considers (for $\Delta f_v = 0$), to the model of Fischer, Appel and co-workers [42,43] for transverse twinning, which was developed to describe the nucleation of transverse twins, in particular on misfit dislocations in the lamellar interfaces based on observations of this by TEM. Only the dissipative term in the Fischer model has been split into two here to describe the dissipative mechanisms intrinsic, τ_D^T, and extrinsic, ξ, to twinning itself.

In the case of the micropillar compression in the present study, the majority of γ-TiAl longitudinal twins were found to be unconstrained. Away from the top of the pillar where local lateral constraint is exerted on the pillar by frictional sliding against the punch, and besides local lattice misfit at the various twin-type interfaces [3], there is no additional elastic energy storage within the pillar beyond the uniform axial elastic strain of the pillar. Daum et al. [44] have evoked the possibility for elastic buckling of lamellae; however, the lamellae are not suitably oriented for buckling in the soft-mode pillars here. None of the lamellae surrounding the twin are required to accommodate a twinning shear and hence $\tau_0 = 0$. Further, to this, as no elastic backstress exists to be relieved by the dissipative mechanisms behind ξ, this must also be null. Eq. (2) now simplifies in the case of unconstrained longitudinal twinning to:

$$\tau_a{}^T = \gamma_T \beta + \tau_D{}^T \tag{3}$$

This expression strongly resembles that produced by Farenc, Couret and co-workers [45] based on *in situ* observations of twinning; the extrinsic energy terms (elastic and plastic accommodation) were not considered. However, Farenc et al. included an extra term describing a thermally activated frictional stress only resisting the movement of the leading twinning partial dislocation, possibly due to covalency effects.

By a similar principle to [19], a variational approach is now taken to assess the temperature dependence of the applied resolved shear stress for twin operation, τ_a^T. The workings of this being both lengthy and partially repetitive of previous analyses of twin formation [19], they are given in Appendix B. The final Eq. (B.7) for the temperature variation at constant strain and strain rate is:

$$\left(\frac{\partial \tau_a{}^T}{\partial T}\right)_{\varepsilon,\dot{\varepsilon}} = \frac{\beta}{\Pi}\left(\frac{\partial \gamma_F}{\partial T}\right)_{\varepsilon,\dot{\varepsilon}} + \frac{\Gamma}{\Pi}\left(\frac{\partial \tau_D{}^T}{\partial T}\right)_{\varepsilon,\dot{\varepsilon}} \tag{4}$$

where in the case of longitudinal twinning of γ-TiAl, the interface energy γ_T has been replaced by the twinning shear fault energy, γ_F, and the terms β, Γ and Π are determined in Appendix B to be positive; Γ and Π depend on the rate of change of β with τ_D^T and τ_a, respectively.

Indeed, the first step in the formation of mechanical twins is the development of a stacking fault that is propagated ahead of the growing twin as the interface with the parent [6]; Kibey et al. [46] further argue that it is the unstable stacking fault energy that dictates the CRSS for twinning in f.c.c metals. Stacking fault energies have been measured on a wide range of metals, often by weak beam imaging of dissociation distances between partial dislocations. Venables has determined the twinning stress in various f.c.c. Cu alloys to vary as the square root of the stacking fault energy [47–49]. This fault energy in f.c.c. structures increases with temperature [17,18]; in h.c.p., the stacking fault energy appears to decrease with temperature [18]. A short explanation for this trend is that the free energy of the f.c.c. structure generally increases with temperature more slowly than that of the h.c.p. structure, such that the f.c.c. stacking of close packed planes is stabilised with increasing temperature relative to the hexagonal-type stacking [18]. The h.c.p. stacking is effectively the local configuration at a stacking fault in an f.c.c. metal. It is tentatively suggested by the authors that the similarities between both twinning and the packing of planes in γ-TiAl and f.c.c. metals results in an equivalent temperature dependence of the twin shear fault energy in γ-TiAl, i.e. increasing with temperature. Further investigation is required to confirm this; the interpretation below of the experimental results does not assume this hypothesis to be valid.

Eq. (4) is vital in understanding the processes that occur during unconstrained longitudinal twinning in the γ-TiAl phase studied here. Indeed as temperature increases from 25 °C to 700 °C, the CRSS for the glide of Shockley partials, τ_D^T, decreases due to the *thermally activated frictional forces* resisting their motion according to an *in situ* study of twin formation [45], similarly to other dislocation mechanisms in Al-lean γ-TiAl, see section 4.2. However, the applied resolved shear stress for twinning, τ_a^T, is experimentally found here to increase with increasing temperature. Hence, for unconstrained longitudinal twinning here to be described by the same energetic approach as Bolling and Richman [19], and Fischer and co-workers [43], the interpretation of the experimental observations is that the twinning shear fault energy γ_F increases with temperature at a faster rate than the corresponding decrease in τ_D^T, weighted by β/Π and Γ/Π respectively.

In short, the temperature dependence of the operation of unconstrained longitudinal twinning in the Ti4522XD alloy is considered to be dominated by the stacking fault energy, the formation of which is a necessary step in the nucleation of a mechanical twin. The temperature dependence of the CRSS is

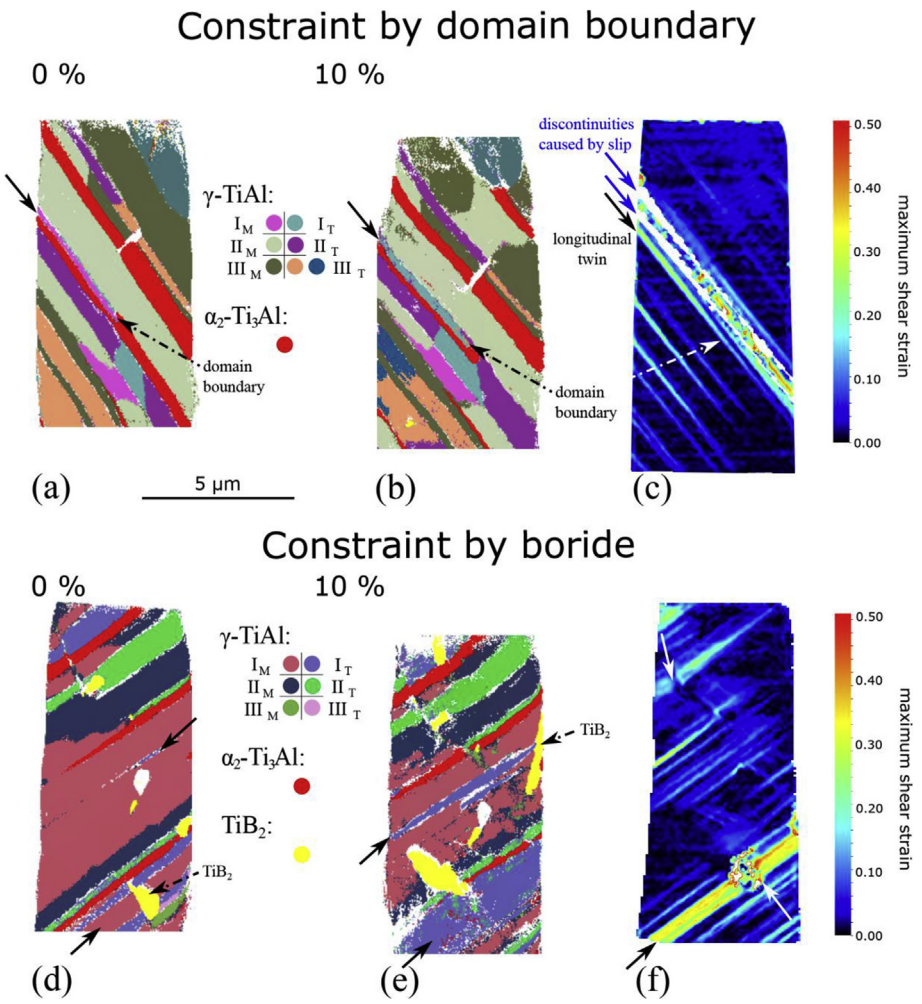

Fig. 8. Effect of constraint on longitudinal twinning: the pre-/post-compression EBSD maps and DIC strain maps for pillars tested at 367 °C, where twinning was constrained by (a–c) a domain boundary and (d–f) a hard TiB_2 particle, are annotated with solid black arrows to indicate the locations of longitudinal twinning and blue arrows to indicate conventional slip. Such constraint was found to increase the resolved shear stress for longitudinal twinning to 171 MPa and 149 MPa, respectively, for the present examples. White arrows in (f) indicate regions where strain uniformity along lamellae is affected by the hard particles. (For interpretation of the references to colour in this figure legend, the reader is referred to the Web version of this article.)

therefore not dominated by the variation in the ease of gliding Shockley partials.

A tension-compression asymmetry (T-CA) is known to exist for the propagation of superdislocations in Al-rich γ-TiAl single crystals at 500–1000 °C [50] due to its asymmetrical dissociation into four Shockley partials; however, single Shockley partials, as found in twinning, are not necessarily susceptible to this T-CA mechanism. Inui et al. have reported an absence of T-CA for two-phase Ti-49.3at.%Al PST crystals [24], although Beran et al. [51] measured a lower twin volume fraction in two-phase Ti-48Al-2Nb-2Cr-0.82B in compression (0.2 vol.%) than in tension (0.3 vol.%) by neutron diffraction upon loading to ±0.2% strain. Mechanical testing in the present study has been undertaken purely in compression, such that any analysis of twinning is appropriate only to twinning in compression; it is possible that the glide of Shockley partials in tension is easier than in compression due to the dislocation core-width effect reported on other systems (e.g. Ni superalloys [52]). This requires further investigation.

4.2. Introducing constraint: comparison with polycrystalline TiAl data

The previous observations [3–5] that the fraction of the γ-TiAl phase that twins increases with temperature in polycrystalline samples across a wide range of test conditions and alloy compositions suggests that twinning in polycrystals becomes easier with increasing temperature.

Where domain boundaries are present, as in section 3.2 and previously [23], the γ-variant undergoing longitudinal twinning is not unconstrained, so the domain boundary that exists in the relevant lamella resists twinning by imparting constraint on the mechanically twinning domain. This causes an increase in the measured CRSS for longitudinal twinning at multiple test temperatures. Ahead of domain boundaries, the twinning shear must be accommodated elastically, both in the neighbouring domain and in the twinned one, or plastically, by dislocation glide ahead of the domain boundary and within the twinning domain. Twinning (transverse or longitudinal) ahead of the domain boundary was not

observed by TEM or by EBSD in previous micropillar work [23] to have occurred as an accommodation mechanism for a longitudinal twin; indeed, the Schmid factor for longitudinal twinning of the neighbouring domain is low or negative [53]. The strain associated with such accommodation has been shown by digital image correlation in Fig. 8 and in Ref. [23] to occur by longitudinal or mixed-mode [2] dislocation glide.

Boride particles may also inhibit twinning, as suggested by the results in section 3.2.1; however, misfit dislocations at precipitate interfaces in TiAl alloys are also known to facilitate twin nucleation (e.g. around perovskites Ti_3AlC [3]), such that the influence of tertiary phases on the ease of twin initiation is not well defined.

In γ-TiAl, the temperature dependence of the CRSS for ordinary dislocations has been found to show anomalous yielding in Al-rich γ-TiAl single crystals [54] although the magnitude varies with composition [3,55,56]. However, further work by Nakano et al. [57] found that below the limiting Al composition for γ-TiAl single crystals, i.e. when a two phase γ-TiAl/α_2-Ti_3Al microstructure is generated (a lamellar one here), the yield stress anomaly disappears and the stress to initiate slip decreases monotonically with temperature between 25 and 700 °C. This was attributed to the destabilisation below a certain Al concentration of nano-scale Al_5Ti_3 precipitates that form as a further ordered superstructure of the γ-TiAl unit cell. The Al_5Ti_3 precipitates require four $\{111\}<1\bar{1}0]$ ordinary γ-TiAl dislocations to pass through a given (111) plane to restore the ordered structure; the anti-phase boundary between them may be stabilised on {001) and {110) planes by cross-slip at higher temperatures, which causes the dislocations to become pinned and hence a yield anomaly to occur. The thermal easing of ordinary dislocation motion in Al-lean γ-TiAl suggests that the resistance to longitudinal twinning due to the constraint of neighbouring domains may decrease with temperature as accommodative plastic flow is facilitated in these neighbouring domains.

In TiAl lamellar polycrystals, the exact aspect ratio of lamellar γ-TiAl domains varies [3], however the simple existence of domain boundaries reflects the fact that for most domains, the majority of their in-plane boundary is with another γ-variant of that colony, rather than being with another colony. Hence the main source of constraint against the longitudinal twinning of a γ domain, by in-plane boundary area, is the neighbouring γ domains. Furthermore, in a separate study, all domains where longitudinal twinning occurred at room temperature in a polycrystalline sample were adjacent to a neighbouring colony at one end [5]. This suggests that colony boundaries are in fact a weaker resistance to longitudinal twinning than domain boundaries. Hence it is not so much a question of the misorientation of neighbouring colonies and whether they are able to accommodate the twinning shear, but rather the resistance of neighbouring domains that determines the magnitude of any constraint.

In a similar fashion to section 4.1, the effect of constraint by neighbouring domains is now incorporated into the mathematical formulation for longitudinal twinning. For this, we return to Eq. (2), setting only $\Delta f_v = 0$ for reasons discussed above. We now retain the elastic resistance of the surrounding material and the twinned material itself to the twinning shear, as well as the possibility for extrinsic energy dissipation, in the case of γ-TiAl by ordinary and super-dislocation motion external and internal to the twin, as well as micro-cracking, to relieve the elastic stresses generated by the twinning shear. Hence:

$$\tau_a{}^T = \tau_0 + \gamma_T\beta + \xi + \tau_D{}^T \tag{5}$$

The development of the variational form of Eq. (5) is given in Appendix C. Approximating the elastic modulus of γ-TiAl to be relatively temperature independent, we obtain from Eq. (C.11):

$$\left(\frac{\partial \tau_a{}^T}{\partial T}\right)_{\varepsilon,\dot{\varepsilon}} = \frac{\beta}{\Omega}\left(\frac{\partial \gamma_F}{\partial T}\right)_{\varepsilon,\dot{\varepsilon}} + \frac{Z}{\Omega}\left(\frac{\partial \tau_y}{\partial T}\right)_{\varepsilon,\dot{\varepsilon}} + \frac{\Psi}{\Omega}\left(\frac{\partial \tau_D{}^T}{\partial T}\right)_{\varepsilon,\dot{\varepsilon}} \tag{6}$$

where β, Z, Ψ and Ω are positive. From our analysis of unconstrained longitudinal twinning, it was concluded that the first term on the right hand side of equation Eq. (6) relating to the twinning shear fault energy should increase with temperature. The latter two, relating to slip processes, ease with increasing temperature, as earlier. Hence, the variation of τ_a^T with temperature is not simply determined. However, the experimental observation that the propensity for longitudinal twinning in lamellar TiAl polycrystals increases significantly between 25 °C and 700 °C [5] indicates that $(\partial \tau_a{}^T/\partial T)_{\varepsilon,\dot{\varepsilon}}$ is negative. In short, when longitudinal twinning is constrained, the temperature variations of the combined extrinsic and intrinsic dislocation processes may now outweigh that of the stacking fault energy, resulting in a decrease with temperature of the applied RSS required for the onset of constrained longitudinal twinning of γ-TiAl.

The result is that it is not just the stacking fault energy, and hence the CRSS of unconstrained twinning, or the ease of gliding Shockley partials to propagate the twin, that determine the propensity for twin formation in polycrystals, as previously suggested; instead, one must also consider the effect of constraint. This constraint is mediated by elasticity and thermally activated dislocation glide in the neighbouring domains and, eventually, in the domain undergoing deformation twinning itself, such that as temperature increases, this constraint is expected to ease. It is likely for this reason that the extent of longitudinal twinning in γ-TiAl, and potentially transverse twinning by equivalent transverse glide mechanisms, increases from 25 °C to 700 °C in bulk, polycrystalline samples.

5. Conclusions

In situ microcompression up to 700 °C of samples milled from single colonies of lamellar Ti-45Al-2Nb-2Mn (at.%)-0.8 vol.% TiB_2, complemented by a combination of EBSD crystal orientation mapping and digital image correlation strain mapping, enabled the critical resolved shear stress for unconstrained longitudinal twinning in γ-TiAl to be measured. It was found to increase monotonically with temperature; this was in agreement with an increased twin shear fault energy with temperature, based on literature models for twin formation. The addition of constraint by γ-variant domain boundaries raised this CRSS. The increased propensity in polycrystals for such mechanical twinning as temperature increases was therefore attributed to an easing of plasticity to reduce constraint by neighbouring domains, rather than an intrinsic softening of deformation twinning of γ-TiAl with increasing temperature.

Acknowledgements

The work was supported by the EPSRC/Rolls-Royce Strategic Partnership (EP/M005607/1). Thanks are due to James Campbell and Alberto Palomares-García for their help with the procedure for minimising sample oxidation during testing. Thanks also to Serge Grop for support with nanoindenter instrumentation. Stefanie Sandlöbes is thanked for fruitful discussions on the thermal evolution of stacking fault energies.

Appendix A. Supplementary data

Supplementary data related to this article can be found at https://doi.org/10.1016/j.actamat.2018.01.007.

Appendices

Appendix A

When the sample heater was heated in closed PID loop to a target of 396 °C measured with a thermocouple embedded in the Cu stub, the TiAl sample surface temperature was found to stabilise at 367 °C. This actual sample surface temperature was measured by using the calibrated diamond tip as a thermometer after calibration indents on the Cu stub. However, when the Cu stub was further heated to 611 °C, the TiAl sample surface temperature was measured to be 633 °C by the same method. The TiAl sample surface temperature was expected to be lower than the Cu stub as the heater is located beneath the stub and TiAl has low thermal conductivity. Attempts to directly measure the TiAl surface temperature using a thermocouple spot-welded to the sample surface were hampered by the thermocouple acting as a heat sink. The anomalous observation is explained below.

In a vacuum, heat transfer to the exposed sample surface from the Cu stub takes place by both conduction and radiation. Before tip-sample contact, heat transfer to the sample from the tip occurs only by radiation. Hence, the rate of heat transfer to the sample, P, from both the stub and the indenter tip is expressed as a function of temperatures, $T_{...}$, of the Cu stub, the diamond tip and the sample as:

$$P = kA_c\left(T_{\text{Cu stub}} - T_{\text{sample}}\right) + \sigma A_{r,\text{Cu stub}}\left({T_{\text{Cu stub}}}^4 - {T_{\text{sample}}}^4\right) + \sigma A_{r,\text{tip}}\left({T_{\text{tip}}}^4 - {T_{\text{sample}}}^4\right) \quad \text{(A.1)}$$

where k is the thermal conductivity of the TiAl alloy, A_c is the area of the sample, σ is the Stefan-Boltzmann constant, and $A_{r,\text{tip}}$ ($A_{r,\text{Cu stub}}$) encompasses both the areas of the sample and tip (Cu stub), their view factor and the respective emissivities of both bodies. The first term on the right hand side of Eq. (A.1) describes conductive heating of the sample, the second is due to radiation from the Cu stub and the third is due to radiation from the indentation tip. The observation that the Cu stub was hotter than the sample at 367 °C, whilst the sample was the hotter at 633 °C and above, indicates an increased contribution of radiative heating from the tip at higher temperatures, such that heating by the Cu stub is no longer solely dominant. Furthermore, such radiative heating from the tip was able to sustain a temperature inversion between the Cu stub and the sample, whereby the $kA_c(T_{\text{Cu stub}} - T_{\text{sample}})$ and $\sigma A_{r,\text{Custub}}({T_{\text{Custub}}}^4 - {T_{\text{sample}}}^4)$ terms are negative.

The thermal conductivity of TiAl alloys in the 25 °C–700 °C range is low for a metal, varying between 22.0 and 27.5 W m^{-1} K^{-1} [3], whereas for Cu it is 401 W m^{-1} K^{-1} at 300 K [58] and for pure Al and Ti it is 237 and 22 W m^{-1} K^{-1} respectively at 300K [58]. Hence, thermal conduction through the sample may have been sufficiently reduced for heat to remain trapped within the sample such that radiative heating by the indentation tip structure could raise the sample surface temperature above that of the Cu stub. Data on the temperature dependence of the emissivity of TiAl alloys was not available to assess the contribution of this to the retention of heat within the sample.

In short, the variation of the sample surface temperature with respect to the sample heater thermocouple embedded in the Cu stub is non-linear for such a sample material. With regards to tip tuning, this means that the usually applied straight line fit of the tip temperature deviation upon contact [25] against the sample heater temperature is no longer valid. For this reason, special care must be taken while performing tip-sample surface temperature tuning. Both coarse tuning with the method in Ref. [25] followed by a more refined tune based on load drift at constant position is recommended to find conditions for isothermal contact.

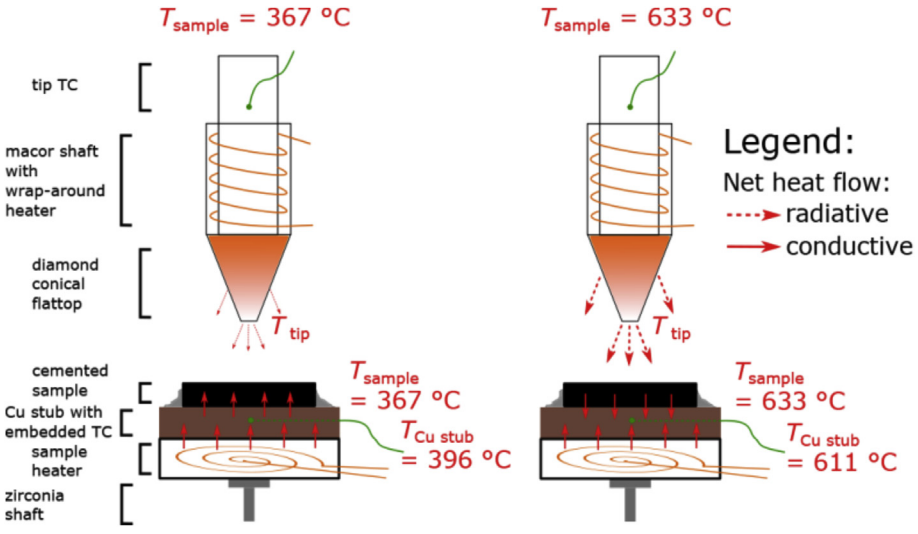

Fig. A.1. Schematic of the heated zone of the *in situ* nano-indenter, indicating local component temperatures for two test temperatures, and the resulting heat transfer (not to scale).

Appendix B

Consider that the terms in Eq. (3) may depend on multiple experimental variables such as temperature, T, strain, ε, and strain rate, $\dot{\varepsilon}$; to generalise, we shall write these variables χ_i, χ_j, χ_k and so on. Now:

$$\left(\frac{\partial {\tau_a}^T}{\partial \chi_i}\right)_{\chi_j,\chi_k\ldots} = \left(\frac{\partial \gamma_T \beta}{\partial \chi_i}\right)_{\chi_j,\chi_k\ldots} + \left(\frac{\partial {\tau_D}^T}{\partial \chi_i}\right)_{\chi_j,\chi_k\ldots} \tag{B.1}$$

so

$$\left(\frac{\partial {\tau_a}^T}{\partial \chi_i}\right)_{\chi_j,\chi_k\ldots} = \gamma_T\left(\frac{\partial \beta}{\partial \chi_i}\right)_{\chi_j,\chi_k\ldots} + \beta\left(\frac{\partial \gamma_T}{\partial \chi_i}\right)_{\chi_j,\chi_k\ldots} + \left(\frac{\partial {\tau_D}^T}{\partial \chi_i}\right)_{\chi_j,\chi_k\ldots} \tag{B.2}$$

and if we consider the possibility, as done in Ref. [19], that β may further vary according to τ_a and τ_D^T, but not τ_0 and τ_y as these are null for unconstrained longitudinal twinning, the following expansion is made:

$$\left(\frac{\partial \beta}{\partial \chi_i}\right)_{\chi_j,\chi_k\ldots} = \left(\frac{\partial \beta}{\partial \tau_a}\right)_{{\tau_D}^T}\left(\frac{\partial \tau_a}{\partial \chi_i}\right)_{\chi_j,\chi_k\ldots} + \left(\frac{\partial \beta}{\partial {\tau_D}^T}\right)_{\tau_a}\left(\frac{\partial {\tau_D}^T}{\partial \chi_i}\right)_{\chi_j,\chi_k\ldots} \tag{B.3}$$

Now Eq. (B.2) is rewritten:

$$\left(\frac{\partial {\tau_a}^T}{\partial \chi_i}\right)_{\chi_j,\chi_k\ldots} = \frac{\beta}{\Pi}\left(\frac{\partial \gamma_T}{\partial \chi_i}\right)_{\chi_j,\chi_k\ldots} + \frac{\Gamma}{\Pi}\left(\frac{\partial {\tau_D}^T}{\partial \chi_i}\right)_{\chi_j,\chi_k\ldots} \tag{B.4}$$

where

$$\Gamma = 1 + \gamma_T\left(\frac{\partial \beta}{\partial {\tau_D}^T}\right)_{\tau_a}$$

$$\Pi = 1 - \gamma_T\left(\frac{\partial \beta}{\partial \tau_a}\right)_{{\tau_D}^T}$$

To determine the temperature dependence of unconstrained longitudinal twinning in γ-TiAl, Γ and Π must be evaluated. If we consider $dA/dV \sim 1/\lambda$ where λ relates a twin thickness, then:

$$\left(\frac{\partial \beta}{\partial {\tau_D}^T}\right)_{\tau_a} = \left(\frac{\partial \beta}{\partial \lambda}\right)_{\tau_a}\left(\frac{\partial \lambda}{\partial {\tau_D}^T}\right)_{\tau_a} \sim -\frac{1}{\varepsilon_s \lambda^2}\left(\frac{\partial \lambda}{\partial {\tau_D}^T}\right)_{\tau_a} > 0 \tag{B.5}$$

$$\left(\frac{\partial \beta}{\partial \tau_a}\right)_{{\tau_D}^T} = \left(\frac{\partial \beta}{\partial \lambda}\right)_{{\tau_D}^T}\left(\frac{\partial \lambda}{\partial \tau_a}\right)_{{\tau_D}^T} \sim -\frac{1}{\varepsilon_s \lambda^2}\left(\frac{\partial \lambda}{\partial \tau_a}\right)_{{\tau_D}^T} < 0 \tag{B.6}$$

Straightforwardly, the twin thickness must increase as the applied stress increases, and as the stress required to activate twin-mediating dislocation glide decreases. Therefore, both Γ and Π are positive; logically β must be also as a twin is created and hence more interfacial area is too, i.e. $dA/dV > 0$.

The application of Eq. (B.4) to the case of temperature variation at constant strain and strain rate gives:

$$\left(\frac{\partial {\tau_a}^T}{\partial T}\right)_{\varepsilon,\dot{\varepsilon}} = \frac{\beta}{\Pi}\left(\frac{\partial \gamma_T}{\partial T}\right)_{\varepsilon,\dot{\varepsilon}} + \frac{\Gamma}{\Pi}\left(\frac{\partial {\tau_D}^T}{\partial T}\right)_{\varepsilon,\dot{\varepsilon}} \tag{B.7}$$

Appendix C

Eq. (5) is expressed in its variational form as in Appendix B as:

$$\left(\frac{\partial {\tau_a}^T}{\partial \chi_i}\right)_{\chi_j,\chi_k\ldots} = \left(\frac{\partial \tau_0}{\partial \chi_i}\right)_{\chi_j,\chi_k\ldots} + \left(\frac{\partial \gamma_T \beta}{\partial \chi_i}\right)_{\chi_j,\chi_k\ldots} + \left(\frac{\partial \xi}{\partial \chi_i}\right)_{\chi_j,\chi_k\ldots} + \left(\frac{\partial {\tau_D}^T}{\partial \chi_i}\right)_{\chi_j,\chi_k\ldots} \tag{C.1}$$

Considering that β and ξ may now depend on τ_a, τ_0, τ_y and τ_D^T, an equivalent process to Appendix B may be executed to obtain:

$$\left(\frac{\partial {\tau_a}^T}{\partial \chi_i}\right)_{\chi_j,\chi_k\ldots} = \frac{\Theta}{\Omega}\left(\frac{\partial \tau_0}{\partial \chi_i}\right)_{\chi_j,\chi_k\ldots} + \frac{\beta}{\Omega}\left(\frac{\partial \gamma_T}{\partial \chi_i}\right)_{\chi_j,\chi_k\ldots} + \frac{Z}{\Omega}\left(\frac{\partial \tau_y}{\partial \chi_i}\right)_{\chi_j,\chi_k\ldots} + \frac{\Psi}{\Omega}\left(\frac{\partial {\tau_D}^T}{\partial \chi_i}\right)_{\chi_j,\chi_k\ldots} \tag{C.2}$$

where

$$\Theta = 1 + \gamma_T\left(\frac{\partial \beta}{\partial \tau_0}\right)_{\tau_a,\tau_y,{\tau_D}^T} + \left(\frac{\partial \xi}{\partial \tau_0}\right)_{\tau_a,\tau_y,{\tau_D}^T}$$

$$Z = \gamma_T\left(\frac{\partial \beta}{\partial \tau_y}\right)_{\tau_a,\tau_0,{\tau_D}^T} + \left(\frac{\partial \xi}{\partial \tau_y}\right)_{\tau_a,\tau_0,{\tau_D}^T}$$

$$\Psi = 1 + \gamma_T\left(\frac{\partial \beta}{\partial {\tau_D}^T}\right)_{\tau_a,\tau_0,\tau_y} + \left(\frac{\partial \xi}{\partial {\tau_D}^T}\right)_{\tau_a,\tau_0,\tau_y}$$

$$\Omega = 1 - \gamma_T\left(\frac{\partial \beta}{\partial \tau_a}\right)_{\tau_0,\tau_y,{\tau_D}^T} - \left(\frac{\partial \xi}{\partial \tau_a}\right)_{\tau_0,\tau_y,{\tau_D}^T}$$

Once again, the derivatives in Θ, Z, Ψ and Ω must be assessed. Eqs. (B.5) and (B.6) still hold equivalently true; additionally,

$$\left(\frac{\partial \beta}{\partial \tau_0}\right)_{\tau_a,\tau_y,{\tau_D}^T} \sim -\frac{1}{\varepsilon_s \lambda^2}\left(\frac{\partial \lambda}{\partial \tau_0}\right)_{\tau_a,\tau_y,{\tau_D}^T} > 0 \tag{C.3}$$

$$\left(\frac{\partial \beta}{\partial \tau_y}\right)_{\tau_a,\tau_0,{\tau_D}^T} \sim -\frac{1}{\varepsilon_s \lambda^2}\left(\frac{\partial \lambda}{\partial \tau_y}\right)_{\tau_a,\tau_0,{\tau_D}^T} > 0 \tag{C.4}$$

These results may be inferred on the same principles as Eqs. (B.5) and (B.6); for a more in-depth explanation, the reader is referred to [19]. The partial derivatives in ξ are as follows:

$$\left(\frac{\partial \xi}{\partial \tau_a}\right)_{\tau_0,\tau_y,{\tau_D}^T} < 1 \tag{C.5}$$

$$\left(\frac{\partial \xi}{\partial \tau_0}\right)_{\tau_a,\tau_y,{\tau_D}^T} > -1 \tag{C.6}$$

$$\left(\frac{\partial \xi}{\partial \tau_y}\right)_{\tau_a,\tau_0,{\tau_D}^T} < 0 \tag{C.7}$$

$$\left(\frac{\partial \xi}{\partial {\tau_D}^T}\right)_{\tau_a,\tau_0,\tau_y} = 0 \tag{C.8}$$

Inequalities (C.5) through (C.7) are justified identically to the treatment of continual mechanical twinning [19]. The additional term here is $(\partial\xi/\partial{\tau_D}^T)_{\tau_a,\tau_0,\tau_y}$ in Eq. (C.8); it is not necessary that the dissipation of energy by extrinsic mechanisms depend on the CRSS for dislocation motion intrinsic to twinning. This may eventually occur in γ-TiAl, e.g. by pinning interaction of twin-mediating Shockley partials with twinning shear-accommodating ordinary dislocations within the twinned region. However, for the initial stages of twinning on which the current study focuses, it is assumed that such dislocation interactions do not yet occur.

Hence, in our evaluation of Θ, Z, Ψ and Ω, we find that Θ, Ψ and Ω are positive. Z is less simple to determine. Unlike the hypothesis for continual mechanical twinning, notably that:

$$\left|\left(\frac{\partial\xi}{\partial\tau_y}\right)_{\tau_a,\tau_0}\right| \gg \left|\gamma_T\left(\frac{\partial\beta}{\partial\tau_y}\right)_{\tau_a,\tau_0}\right|$$

such that it is a twin propagation-controlled process, the present description for longitudinal twinning requires the hypothesis:

$$\left|\left(\frac{\partial\xi}{\partial\tau_y}\right)_{\tau_a,\tau_0}\right| \ll \left|\gamma_T\left(\frac{\partial\beta}{\partial\tau_y}\right)_{\tau_a,\tau_0}\right| \tag{C.9}$$

or, in the very least:

$$\left|\left(\frac{\partial\xi}{\partial\tau_y}\right)_{\tau_a,\tau_0}\right| < \left|\gamma_T\left(\frac{\partial\beta}{\partial\tau_y}\right)_{\tau_a,\tau_0}\right| \tag{C.10}$$

such that according to the extrema analysis by Bolling and Richman, the mechanism be nucleation-limited [19], as previously reported for longitudinal twinning in γ-TiAl [23]. Hence, Z is positive.

Finally, expressing Eq. (C.2) in terms of the temperature dependence of the applied resolved shear stress for constrained longitudinal twinning, and approximating the elasticity of γ-TiAl to be relatively temperature independent, we obtain:

$$\left(\frac{\partial{\tau_a}^T}{\partial T}\right)_{\varepsilon,\dot{\varepsilon}} = \frac{\beta}{\Omega}\left(\frac{\partial\gamma_T}{\partial T}\right)_{\varepsilon,\dot{\varepsilon}} + \frac{Z}{\Omega}\left(\frac{\partial\tau_y}{\partial T}\right)_{\varepsilon,\dot{\varepsilon}} + \frac{\Psi}{\Omega}\left(\frac{\partial{\tau_D}^T}{\partial T}\right)_{\varepsilon,\dot{\varepsilon}} \tag{C.11}$$

where β, Z, Ψ and Ω are positive.

References

[1] E. Goo, Application of von Mises criterion to single and dual phase TiAl, Scripta Mater. 38 (11) (1998) 1711–1716.
[2] R. Lebensohn, H. Uhlenhut, C. Hartig, H. Mecking, Plastic flow of γ-TiAl-based polysynthetically twinned crystals: micromechanical modeling and experimental validation, Acta Mater. 46 (13) (1998) 4701–4709.
[3] F. Appel, J.D.H. Paul, M. Oehring, Gamma Titanium Aluminide Alloys : Science and Technology, Wiley-VCH, Weinheim, 2011.
[4] F. Appel, R. Wagner, M. Yoo, M. Wuttig, Twinning in advanced materials, in: M.H. Yoo, M. Wuttig (Eds.), TMS Symp. Proc., 1994, pp. 317–330. Warrendale, PA.
[5] T.E.J. Edwards, F. Di Gioacchino, R. Muñoz-Moreno, W.J. Clegg, The interaction of borides and longitudinal twinning in polycrystalline TiAl alloys, Acta Mater. 140 (Supplement C) (2017) 305–316.
[6] J.W. Christian, S. Mahajan, Deformation twinning, Prog. Mater. Sci. 39 (1–2) (1995) 1–157.
[7] M. Yoo, Deformation twinning in superlattice structures, J. Mater. Res. 4 (01) (1989) 50–54.
[8] M.H. Yoo, C.L. Fu, Physical constants, deformation twinning, and microcracking of titanium aluminides, Metall. Mater. Trans. 29 (1) (1998) 49–63.
[9] C.L. Fu, M.H. Yoo, Elastic constants, fault energies, and dislocation reactions in TiAl: a first-principles total-energy investigation, Phil. Mag. Lett. 62 (3) (1990) 159–165.
[10] C. Woodward, J. MacLaren, S. Rao, Electronic structure of planar faults in TiAl, J. Mater. Res. 7 (07) (1992) 1735–1750.
[11] W.J. Zhang, F. Appel, Effect of Al content and Nb addition on the strength and fault energy of TiAl alloys, Mater. Sci. Eng. 329–331 (2002) 649–652.
[12] X.P. Song, G.L. Chen, Determination of the stacking fault energy in high-Nb γ-TiAl, J. Mater. Sci. Lett. 20 (7) (2001) 659–661.
[13] Y.F. Wen, J. Sun, Generalized planar fault energies and mechanical twinning in gamma TiAl alloys, Scripta Mater. 68 (9) (2013) 759–762.
[14] F. Appel, An electron microscope study of mechanical twinning and fracture in TiAl alloys, Phil. Mag. 85 (2–3) (2005) 205–231.
[15] M.H. Yoo, On the dislocation pole mechanism for twinning in TiAl crystals, Phil. Mag. Lett. 76 (4) (1997) 259–268.
[16] A. Couret, S. Farenc, D. Caillard, A. Coujou, M. Yoo, M. Wuttig, Twinning in advanced materials, in: M.H. Yoo, M. Wuttig (Eds.), TMS Symp. Proc., TMS, Warrendale, PA, 1994, pp. 361–374.
[17] P.C.J. Gallagher, The influence of alloying, temperature, and related effects on the stacking fault energy, Metall. Trans. 1 (9) (1970) 2429–2461.
[18] L. Rémy, A. Pineau, B. Thomas, Temperature dependence of stacking fault energy in close-packed metals and alloys, Mater. Sci. Eng. 36 (1) (1978) 47–63.
[19] G.F. Bolling, R.H. Richman, Continual mechanical twinning, Acta Metall. 13 (7) (1965) 709–722.
[20] S. Mahajan, D.F. Williams, Deformation twinning in metals and alloys, Int. Metall. Rev. 18 (2) (1973) 43–61.
[21] A. Jain, S.R. Agnew, Modeling the temperature dependent effect of twinning on the behavior of magnesium alloy AZ31B sheet, Mater. Sci. Eng. 462 (1–2) (2007) 29–36.
[22] L. Straka, A. Soroka, H. Seiner, H. Hänninen, A. Sozinov, Temperature dependence of twinning stress of Type I and Type II twins in 10M modulated Ni–Mn–Ga martensite, Scripta Mater. 67 (1) (2012) 25–28.
[23] T.E.J. Edwards, F. Di Gioacchino, R. Muñoz-Moreno, W.J. Clegg, Deformation of lamellar TiAl alloys by longitudinal twinning, Scripta Mater. 118 (2016) 46–50.
[24] H. Inui, M.H. Oh, A. Nakamura, M. Yamaguchi, Room-temperature tensile deformation of polysynthetically twinned (PST) crystals of TiAl, Acta Metall. Mater. 40 (11) (1992) 3095–3104.
[25] J.M. Wheeler, P. Brodard, J. Michler, Elevated temperature, in situ indentation with calibrated contact temperatures, Phil. Mag. 92 (25–27) (2012) 3128–3141.
[26] J.M. Wheeler, J. Michler, Elevated temperature, nano-mechanical testing in situ in the scanning electron microscope, Rev. Sci. Instrum. 84 (4) (2013), 045103.
[27] G. Mohanty, J. Wehrs, B.L. Boyce, A. Taylor, M. Hasegawa, L. Philippe, J. Michler, Room temperature stress relaxation in nanocrystalline Ni measured by micropillar compression and miniature tension, J. Mater. Res. 31 (8) (2016) 1085–1095.
[28] P.A. Shade, R. Wheeler, Y.S. Choi, M.D. Uchic, D.M. Dimiduk, H.L. Fraser, A combined experimental and simulation study to examine lateral constraint effects on microcompression of single-slip oriented single crystals, Acta Mater. 57 (15) (2009) 4580–4587.
[29] F. Di Gioacchino, W.J. Clegg, Mapping deformation in small-scale testing, Acta Mater. 78 (2014) 103–113.
[30] J.C. Stinville, M.P. Echlin, P.G. Callahan, V.M. Miller, D. Texier, F. Bridier, P. Bocher, T.M. Pollock, Measurement of strain localization resulting from monotonic and cyclic Loading at 650 °C in nickel base superalloys, Exp. Mech. 57 (2017) 1289–1309.
[31] T.E.J. Edwards, F. Di Gioacchino, H.P. Springbett, R.A. Oliver, W.J. Clegg, Stable speckle patterns for nano-scale strain mapping up to 700 °C, Exp. Mech. 57 (2017) 1469–1482.
[32] A.J. Palomares-García, M.T. Pérez-Prado, J.M. Molina-Aldareguia, Effect of lamellar orientation on the strength and operating deformation mechanisms of fully lamellar TiAl alloys determined by micropillar compression, Acta Mater. 123 (2017) 102–114.
[33] K. Fujimura, K. Kishida, K. Tanaka, H. Inui, Compression of micropillars of TiAl coexisting with Ti3Al, MRS Online Proc. Libr. 1295 (2011) 201–206.
[34] T. Fujiwara, A. Nakamura, M. Hosomi, S.R. Nishitani, Y. Shirai, M. Yamaguchi, Deformation of polysynthetically twinned crystals of TiAl with a nearly stoichiometric composition, Philos. Mag. A 61 (4) (1990) 591–606.
[35] T.A. Parthasarathy, M.G. Mendiratta, D.M. Dimiduk, Flow behavior of PST and fully lamellar polycrystals of Ti–48Al in the microstrain regime, Acta Mater. 46 (11) (1998) 4005–4016.
[36] Y. Peng, F. Chen, M. Wang, X. Su, G. Chen, Relationship between mechanical properties and lamellar orientation of PST crystals in Ti-45Al-8Nb alloy, Acta Metall. Sin. 49 (11) (2013) 1457–1461.
[37] Y.L. Chiu, P. Penhoud, P. Veyssière, Portevin-Le Chatelier instability in a L10-TiAl single crystal, Int. J. Mod. Phys. B 20 (25n27) (2006) 4189–4194.
[38] U. Messerschmidt, M. Bartsch, S. Guder, D. Häußler, R. Haushälter, M. Yamaguchi, Dynamic dislocation behaviour in the intermetallic compounds NiAl, TiAl and MoSi2, Intermetallics 6 (7) (1998) 729–733.
[39] H.J. Frost, M.F. Ashby, Deformation-mechanism Maps: the Plasticity and Creep of Metals and Ceramics, Pergamon Press, 1982.
[40] U. Fröbel, F. Appel, Strain ageing in γ(TiAl)-based titanium aluminides due to antisite atoms, Acta Mater. 50 (14) (2002) 3693–3707.
[41] B.A. Simkin, B.C. Ng, M.A. Crimp, T.R. Bieler, Crack opening due to deformation twin shear at grain boundaries in near-γ TiAl, Intermetallics 15 (1) (2007) 55–60.
[42] H. Petryk, F.D. Fischer, W. Marketz, H. Clemens, F. Appel, An energy approach to the formation of twins in TiAl, Metall. Mater. Trans. 34 (12) (2003) 2827–2836.
[43] M. Rester, F.D. Fischer, C. Kirchlechner, T. Schmoelzer, H. Clemens, G. Dehm, Deformation mechanisms in micron-sized PST TiAl compression samples:

experiment and model, Acta Mater. 59 (9) (2011) 3410–3421.
[44] B. Daum, G. Dehm, H. Clemens, M. Rester, F.D. Fischer, F.G. Rammerstorfer, Elastoplastic buckling as source of misinterpretation of micropillar tests, Acta Mater. 61 (13) (2013) 4996–5007.
[45] S. Farenc, A. Coujou, A. Couret, An in situ study of twin propagation in TiAl, Philos. Mag. A 67 (1) (1993) 127–142.
[46] S. Kibey, J.B. Liu, D.D. Johnson, H. Sehitoglu, Predicting twinning stress in fcc metals: linking twin-energy pathways to twin nucleation, Acta Mater. 55 (20) (2007) 6843–6851.
[47] J.A. Venables, Deformation twinning in face-centred cubic metals, Phil. Mag. 6 (63) (1961) 379–396.
[48] J.A. Venables, Deformation twinning in fcc metals, in: R.E. Reed-Hill, J.P. Hirth, H.C. Rogers (Eds.), AIME Conference Deformation Twinning, Gordon & Breach, Gainesville, Florida, USA, 1963.
[49] M.A. Meyers, O. Vöhringer, V.A. Lubarda, The onset of twinning in metals: a constitutive description, Acta Mater. 49 (19) (2001) 4025–4039.
[50] M. Zupan, K.J. Hemker, Yielding behavior of aluminum-rich single crystalline γ-TiAl, Acta Mater. 51 (20) (2003) 6277–6290.
[51] P. Beran, M. Heczko, T. Kruml, T. Panzner, S. van Petegem, Complex investigation of deformation twinning in γ-TiAl by TEM and neutron diffraction, J. Mech. Phys. Solid. 95 (2016) 647–662.
[52] F.E. Heredia, D.P. Pope, The tension/compression flow asymmetry in a high γ' volume fraction nickel base alloy, Acta Metall. 34 (2) (1986) 279–285.
[53] V. Paidar, K. Kishida, M. Yamaguchi, Polarization of plastic deformation modes in polysynthetically twinned TiAl crystals, J. Mater. Res. 18 (3) (2011) 702–708.
[54] T. Kawabata, T. Kanai, O. Izumi, Positive temperature dependence of the yield stress in TiAl L10 type superlattice intermetallic compound single crystals at 293–1273 K, Acta Metall. 33 (7) (1985) 1355–1366.
[55] H. Inui, M. Matsumuro, D.H. Wu, M. Yamaguchi, Temperature dependence of yield stress, deformation mode and deformation structure in single crystals of TiAl (Ti–56 at.% Al), Philos. Mag. A 75 (2) (1997) 395–423.
[56] T. Nakano, K. Hayashi, Y. Umakoshi, Y.L. Chiu, P. Veyssière, Effects of Al concentration and resulting long-period superstructures on the plastic properties at room temperature of Al-rich TiAl single crystals, Phil. Mag. 85 (22) (2005) 2527–2548.
[57] T. Nakano, K. Hagihara, T. Seno, N. Sumida, M. Yamamoto, Y. Umakoshi, Stress anomaly in Al-rich Ti-Al single crystals deformed by the motion of 1/2«110] ordinary dislocations, Phil. Mag. Lett. 78 (5) (1998) 385–391.
[58] N.A. Lange, J.A. Dean, Lange's Handbook of Chemistry, McGraw-Hill, 1979.
[59] C. Zambaldi, Micromechanical Modeling of Gamma-TiAl Based Alloys, RWTH Aachen, 2010.